

Original Research

Three-dimensional segmentation and depth-encoded visualization of choroidal vasculature using swept-source optical coherence tomography

Hao Zhou¹ , Tommaso Bacci^{2,3}, K Bailey Freund^{2,3} and Ruikang K Wang^{1,4}

¹Department of Bioengineering, University of Washington, Seattle, WA 98105, USA; ²Vitreous Retina Macula Consultants of New York, New York 10022, USA; ³Department of Ophthalmology, New York University Grossman School of Medicine, New York 10016, USA;

⁴Department of Ophthalmology, University of Washington, Seattle, WA 98105, USA

Corresponding author: Ruikang K Wang. Email: wangrk@uw.edu

Impact statement

The choroid plays an essential role in the pathogenesis of many retinal disorders. Traditional imaging techniques used to visualize the choroid, including indocyanine green angiography, are often invasive and typically lack depth-resolved information. Herein, swept-source optical coherence tomography (SS-OCT) imaging methods are applied to visualize full-thickness choroidal structure and investigate its topographical features and choroidal thickness. Our technique encodes full-thickness choroidal slabs obtained with SS-OCT into three-dimensional (3D) networks of choroidal vessels, enabling *in vivo* visualization of individual choroidal vessels that provides potential for more precise quantitative analysis when compared to other choroidal imaging techniques. This improved visualization of choroidal vasculature structure may prove useful in providing greater insight into the choroid's role in several of the most important causes of vision loss including age-related and myopic degeneration, diabetic retinopathy, and pachychoroid diseases.

Abstract

The choroid provides nutritional support for the retinal pigment epithelium and photoreceptors. Choroidal dysfunction plays a major role in several of the most important causes of vision loss including age-related macular degeneration, myopic degeneration, and pachychoroid diseases such as central serous chorioretinopathy and polypoidal choroidal vasculopathy. We describe an imaging technique using depth-resolved swept-source optical coherence tomography (SS-OCT) that provides full-thickness three-dimensional (3D) visualization of choroidal anatomy including topographical features of individual vessels. Enrolled subjects with different clinical manifestations within the pachychoroid disease spectrum underwent 15 mm × 9 mm volume scans centered on the fovea. A fully automated method segmented the choroidal vessels using their hyporeflective lumens. Binarized choroidal vessels were rendered in a 3D viewer as a vascular network within a choroidal slab. The network of choroidal vessels was color depth-encoded with a reference to the Bruch's membrane segmentation. Topographical features of the choroidal vasculature were characterized and compared with choroidal imaging obtained with indocyanine green angiography (ICGA) from the same subject. The *en face* SS-OCT projections of the larger choroid vessels closely resembled to that obtained with ICGA, with the automated SS-OCT approach providing additional depth-encoded 3D information. In 16 eyes with pachychoroid disease, the SS-OCT approach added clinically relevant structural details, including choroidal thickness and vessel depth, which the ICGA studies could not provide. Our technique

appears to advance the *in vivo* visualization of the full-thickness choroid, successfully reveals the topographical features of choroidal vasculature, and shows potential for further quantitative analysis when compared with other choroidal imaging techniques. This improved visualization of choroidal vasculature and its 3D structure should provide an insight into choroid-related disease mechanisms as well as their responses to treatment.

Keywords: Depth-encoded choroid visualization, choroid imaging, 3D data, swept-source optical coherence tomography

Experimental Biology and Medicine 2021; 246: 2238–2245. DOI: 10.1177/15353702211028540

Introduction

Improved *in vivo* imaging of choroidal structure has been of great clinical interests for decades due to the choroid's critical role in common ocular diseases causing vision loss.^{1,2} Located below the retina and anterior to the sclera, the choroid is a tissue layer composed of blood vessels and stroma that is mainly responsible for delivering nutrients and supporting the metabolic exchange between the systemic circulation and the retinal pigment epithelium (RPE) and photoreceptors. The choroid contributes blood flow to the retina and optic nerve and maintains ocular thermoregulation.^{3–5} Choroidal blood flow accounts for 85% of all ocular blood flow, and choroidal dysfunction is strongly implicated in many ocular diseases including age-related macular degeneration, myopic degeneration, inherited retinal degenerations, and central serous chorioretinopathy (CSC).^{5,6} Because the choroid is located beneath the RPE and Bruch's membrane (BrM), several anatomical and physiological compartments need to be crossed before choroid can be visualized with optical imaging devices.⁷ Traditional clinical imaging technologies using short optical wavelengths including fundus autofluorescence and fluorescein angiography fail to image the full-thickness choroid due to light absorption by pigment in the photoreceptors, RPE, and within the choroid.^{8,9} Multispectral imaging has been explored to selectively image retinal and choroidal structures in traditional fundus photography. Studies have shown that the retina is sensitive to visible light, while the choroid can be imaged with near infrared light.^{10–12} Indocyanine green angiography (ICGA) utilizes deeper penetrating longer wavelengths capable of imaging the choroid's full thickness; however, ICGA provides 2D images lacking depth information.¹³ Moreover, ICGA is an invasive test with rare, but potentially, serious adverse reactions to the intravenous dye.¹⁴ Optical coherence tomography (OCT) is a non-invasive imaging technique providing high-resolution depth-resolved images of ocular structures. Recent advances in OCT technology permit the rapid acquisition of dense volume scans which, when rendered in three dimensional (3D), enable functional ocular imaging.¹⁵ Spectral domain OCT (SD-OCT) utilizes a technique called enhanced-depth imaging to mitigate the sensitivity roll off limitation, which enhances the measurement sensitivity for the structures below the RPE/BrM complex.¹⁶ Swept-source optical coherence tomography (SS-OCT) uses a frequency swept laser that enables interference measurements at different optical frequencies or sequentially over time. This significantly improves penetration of the sampling beam and signal fall-off compared to SD-OCT.^{17,18} By using a longer wavelength of light, SS-OCT has been shown to provide superior choroidal imaging than SD-OCT.¹⁵

Despite recent progress using SS-OCT for choroidal imaging, methods for segmentation and visualization of individual choroidal vessels from SS-OCT scans remain limited.^{6,15} To date, studies using SS-OCT to study the choroid have measured choroid thickness on individual B-scans or over the entire scanning region.^{19–24} However, since choroid thickness may be influenced by factors such

as interstitial fluid and inflammatory infiltration, choroidal thickness measurements may not accurately reflect choroidal blood volume.

Choroidal vessels appear as dark lumens in *en face* OCT choroidal slabs. Choroidal vascularity index (CVI) is typically calculated as the area ratio in a small subfoveal region at a limited number of locations or along a relatively small number of B-scans.^{25,26} Although the CVI is potentially useful to quantify choroidal vascular density, it cannot reveal topographical features of individual choroidal vessels.^{27,28} While in some diseases, choroidal thickness and morphology of individual choroidal vessels may be atypical throughout the entire choroid, in others there may be focal or regional differences in these features.^{29,30} 3D visualization of the choroid would be more likely to identify and quantify this local variability.

Challenges in complicated preprocessing efforts, dependence on modeling, heavy computational labor, and availability of a user-friendly 3D viewer have prevented researchers and clinicians from accessing the benefits of 3D choroidal visualization.^{27,31–36} In our preliminary study, we pioneered an attenuation correction-assisted method to automatically quantify the choroid using the entire SS-OCT 3D dataset.³⁷ This strategy was shown to increase the inter-layer contrast, enabling more accurate segmentation of choroid and choroid vessels, and minimizing the shadowing effects from large retinal vessels.^{37,38} To achieve an easy-to-access *in vivo* visualization of choroidal vasculature, herein we introduce an innovative approach to segment choroidal vessels and automatically present the binarized choroidal vessel network in a 3D viewer. In addition to visualization of vessel anatomy, we show that additional information may be mapped on the vessel's surface. Since choroid thickness is a key metric in evaluating choroid-related eye diseases, we added color-coded depth information indicating the distance from the choroidal vessel surface to BrM. The choroidal vessels are presented in a 3D reconstruction of the choroidal vasculature in which vascular depth can be directly visualized.

Materials and methods

Subjects and choroid imaging

Patients were enrolled in a prospective SS-OCT imaging study approved by Western Institutional Review Board (Olympia, WA). Informed consent was obtained from each subject before imaging. The study was performed in accordance with the tenets of the Declaration of Helsinki and complied with the Health Insurance Portability and Accountability Act of 1996.

SS-OCT and ICGA images of the eye with most evident clinical manifestations in subjects with pachychoroid disease were selected for the present analysis. Patients were diagnosed as having pachychoroid disease if presenting with characteristics referable to conditions within the pachychoroid disease spectrum in at least one eye, as evaluated using a complex of clinical and multimodal imaging parameters.³⁰ Widefield ICGA images were acquired (Optos California, Dunfermline, Scotland, UK) on the

same day of the SS-OCT study. Early-to-mid-phase ICGA of the detailed choroidal vasculature were screened, and the best angiograms were used for image analysis. OCT data were acquired by a commercial SS-OCT system (PlexElite 9000, Carl Zeiss Meditec Inc.). The central wavelength of the light source is 1050 nm with a bandwidth of 100 nm, yielding a full width of half maximum axial resolution of $\sim 5\ \mu\text{m}$ in tissue and a lateral resolution of $\sim 20\ \mu\text{m}$ at the surface of retina. The A-scan scanning rate is 100 kHz and the A-scan depth is 3.0 mm in tissue sampled with 1536 pixels. The scanning protocol is $15\ \text{mm} \times 9\ \text{mm}$, which consisted of 834 B-scans (slow 15 mm scan), and each B-scan consisted of 500 A-scans (fast 9 mm scan). This SS-OCT prototype is equipped with FastTracTM motion correction software to reduce motion artifacts.³⁹ Scans with signal intensity less than 7 were excluded according to the manufacturer's instructions.

Choroid vessel segmentation

Choroid vessels were segmented from the 3D SS-OCT dataset using a previously published method.³⁷ Attenuation correction was first applied to eliminate the projection artifacts from retinal vessels and to enhance the contrast of choroid layer (Figure 1(a) and (b)). On each B-scan, the choroidal slab was segmented from BrM to the outer boundary of choroidal vessels using an automated graph search-based algorithm. The candidate nodes were firstly searched at the inflexion points in the vertical direction where OCT signals change from dark to bright at the vessel bottoms and then selected for the shortest path across the bottom

of choroidal vessels.³⁷ Choroidal vessels were further segmented from the choroidal slab using Otsu's binarization method (Figure 1(c)). Values of pixels in the OCT dataset were assigned as

$$B_{(x,y,z)} = \begin{cases} 1, & \text{choroidal vessel} \\ 0, & \text{non-choroidal vessel} \end{cases} \quad (1)$$

where (x, y, z) was the location of each pixel in the 3D dataset. All the binarized choroidal vessels were re-assembled into 3D network, which can be visualized using ImageJ (National Institutes of Health, Bethesda, Maryland, USA; available at <http://rsb.info.nih.gov/ij/index.html>) 3D viewer (Figure 1(e) to (g)).

En face choroidal vasculature

En face image of choroidal vasculature was generated by sum projection of the binarized choroidal vessels in 3D dataset. Histogram was redistributed to adjust the contrast for better presentation of small vessels by

$$I = I_{min} + \sqrt{2\beta^2 \ln\left(\frac{1}{1 - P(I'_{en\ face})}\right)} \quad (2)$$

where I is the output intensity, I' is the input intensity, I_{min} is the low bound, P is the cumulative probability of the input, and β is the Rayleigh parameter (Details of the MatLab function can be found from the following link: <http://www.mathworks.com/help/matlab/ref/raylmap.html>)

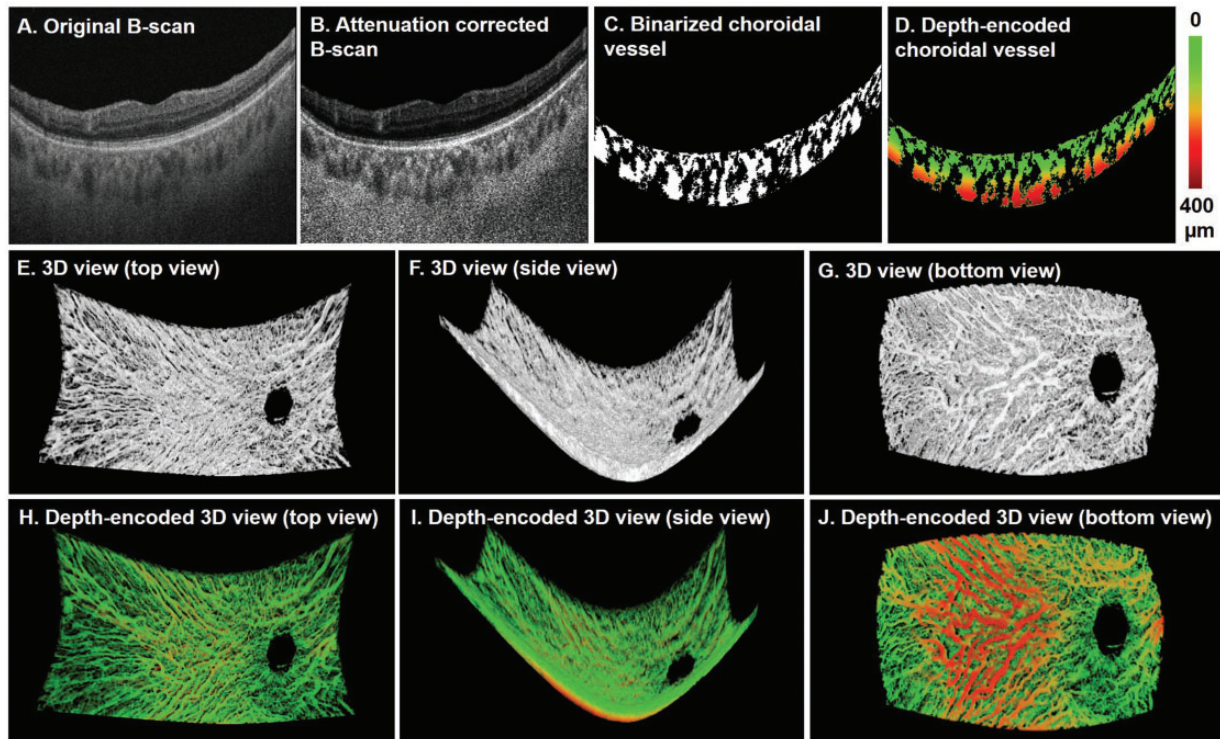


Figure 1. Depth-encoded 3D visualization of choroid vessels. Attenuation correction was applied to the original SS-OCT scan (a and b). Choroidal vessels were segmented, binarized (c) and color-coded using the distance to BrM (d). The reassembled 3D choroidal vessel network without (e to g) and with depth-encoding (h to j) was visualized using the ImageJ 3D viewer with top view, side view and bottom view from left to right, respectively. (A color version of this figure is available in the online journal.)

<https://www.mathworks.com/help/images/ref/adapthisteq.html>). Histogram equalization increases the global contrast by uniformizing the histogram of the images.⁴⁰

Depth-encoded choroidal vessel

The distance of choroidal vessel to the BrM was color-coded via

$$D_{(x,y,z)} = (z - z_{BrM}) \times B_{(x,y,z)} \quad (3)$$

where $D_{(x,y,z)}$ is the value of each pixel at (x, y, z) and z_{BrM} is the location of BrM in the corresponding A-scan at (x, y) (Figure 1(d)). The depth information can be visualized as a RGB color through the ImageJ 3D viewer (Figure 1(h) to (j)). Vessels that were closer to BrM were presented in green while vessels closer to the choroid-scleral junction were colored red.

3D visualization of choroid vessels

The choroidal vasculature can be visualized at any angle in the ImageJ 3D viewer. Figure 1(e) to (j) shows representative images of views from the anterior vitreous (top view, Figure 1(e) and (h)), from the peripheral retina

(side view, Figure 1(f) and (i)) or from the sclera (bottom view, Figure 1(g) and (j)).

Results

We initially analyzed the agreement of choroidal imaging between SS-OCT and ICGA. Sixteen eyes underwent SS-OCT and ICGA imaging, and each was imaged on the same day. Statistical analysis on the repeatability of segmentation and its correlation with aging in normal eyes has been studied in our previous work.³⁸ *En face* images of the choroid vasculature were generated via sum projection of the vessels and compared with the same region cropped from a corresponding ICGA image (Figure 2). Due to the complexity of comparing resolution and correcting distortion in the two types of images, quantitative comparison was not attempted. Instead, skeletons of the major vessels visualized in the *en face* SS-OCT image were manually drawn by experts (first by HZ, and then confirmed by RKW and KBF) overlaid on the ICGA image. We observed similar patterns for the major branches of choroidal vessels in both SS-OCT and ICGA imaging in all 16 eyes.

The depth-encoded 3D visualization of choroidal vasculature provided: (1) the proportion of the choroid volume occupied by vessels; (2) a curved BrM surface; (3) curved

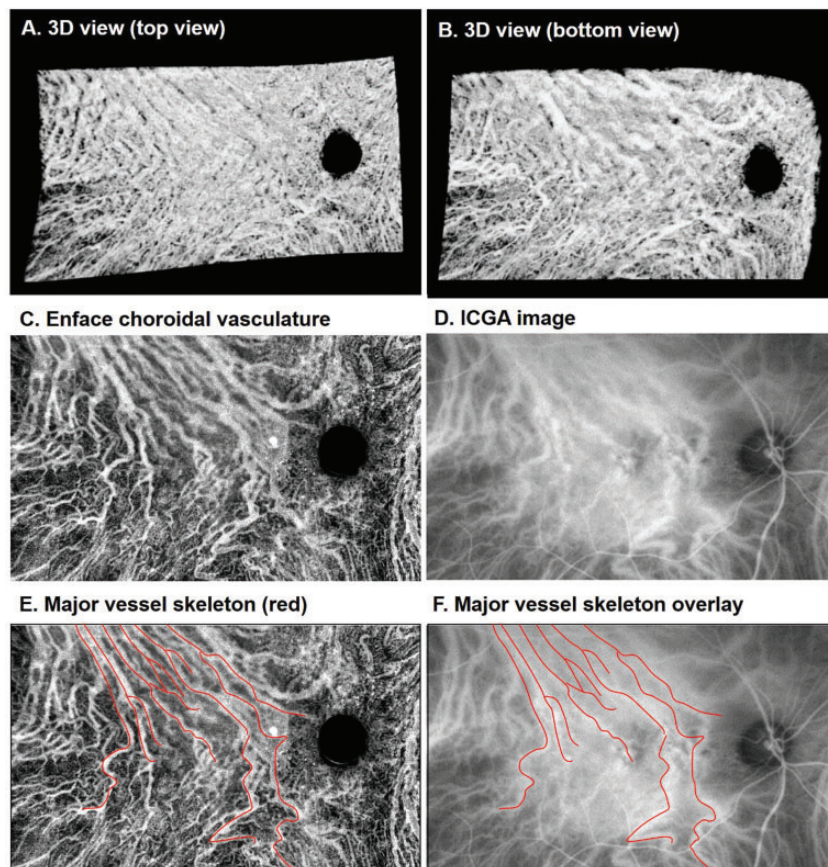


Figure 2. Comparison of choroidal vasculature obtained from SS-OCT and ICGA. (a and b) 3D view of the choroid from a 75-year-old female patient with central serous chorioretinopathy. (c) *En face* images of choroidal vasculature generated via sum projection. (d) Cropped ICGA image at the same region. (e) Skeleton of major choroidal vessels (red) manually drawn on the *en face* image (c). (f) ICGA image with the vessel skeleton overlaid. (A color version of this figure is available in the online journal.)

ICGA: indocyanine green angiography.

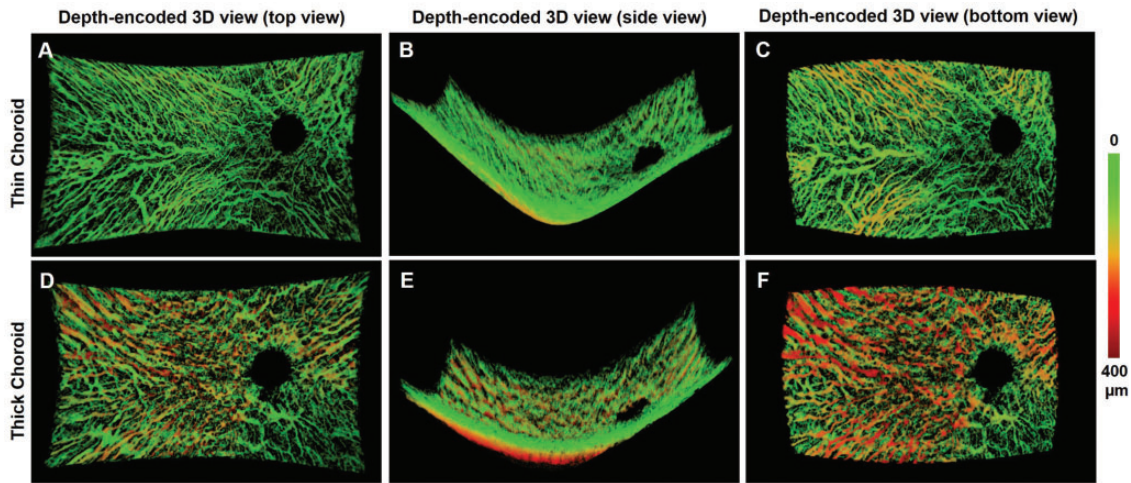


Figure 3. Examples of depth-encoded 3D visualization of a thin (Top row) and thick (Bottom row) choroid. Top views from the vitreous (a and d), side views from the peripheral (b and e), and bottom views from the sclera (c and f) were obtained from the 3D view of an eye with thin choroid (Top row), and an eye with thick choroid (Bottom row), respectively. (A color version of this figure is available in the online journal.)

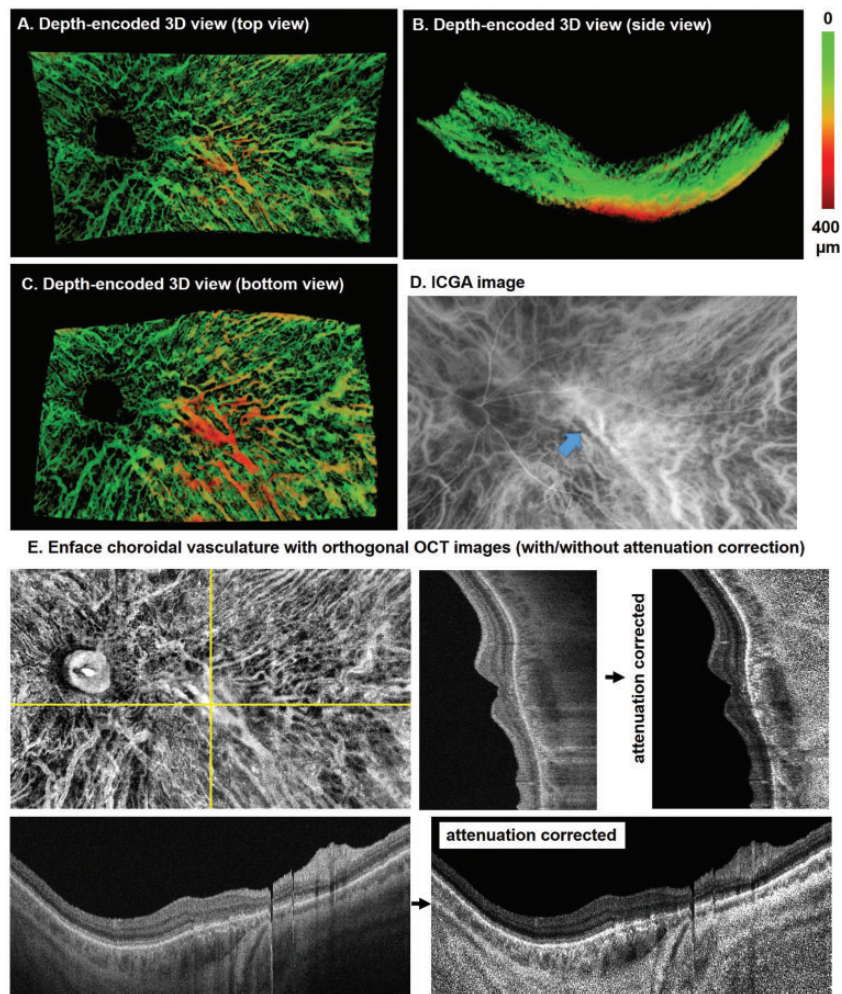


Figure 4. An example of depth-encoded 3D visualization of choroid vessels in the left eye of a 71-year-old male with resolved central serous chorioretinopathy. Top view from the vitreous (a), side view from the peripheral retina (b), and bottom view from the sclera (c) show the choroidal vessels segmented from SS-OCT dataset. (d) The corresponding ICGA image shows a large choroidal vessel passing through macula (arrow). (e) *En face* choroidal vasculature map with orthogonal SS-OCT images shown with and without attenuation correction. (A color version of this figure is available in the online journal.) ICGA: indocyanine green angiography; OCT: optical coherence tomography.

choroid-scleral interface; (4) an appreciation of connectivity between individual vessels within the vascular network; (5) visualization of choroidal thickness throughout the volume. Figure 3 shows examples of 3D views of an eye with a thin choroid and an eye with a thick choroid. Vessels that were more than $150\ \mu\text{m}$ away from BrM were presented in yellow to red color at the bottom. Choroidal vessels of medium size found mostly in Sattler's layer were seen best in the top view, while larger choroidal vessels typically present in Haller's layer were best seen from the bottom view. Side views provided the curvature of both BrM and choroid-scleral junction (Figure 3(b) and (e)). Branching vessels from the large vessels appeared more frequently in the top view than in the bottom view.

Figure 4 shows a depth-encoded 3D visualization of choroid vessels in the left eye of a 71-year-old man with CSC. OCT B-scans show retinal thinning and outer retinal disruption subsequent to resorption of long-lasting subretinal

fluid in the context of CSC (Figure 4). Most of the choroidal vessels in this eye are confined to a superficial thin layer, which is shown as a green network. A large vein located in the outer choroid of the macular region appears in red (bottom view, Figure 4(c)). A similar vascular morphology is observed in ICGA images; however, the depth of the large vein passing through macula and draining into the inferotemporal vortex vein cannot be determined (Figure 4(d)). From the corresponding SS-B-scans, we also observed the large dark lumen beneath the macula near the choroid-scleral junction that corresponds to the large vein (Figure 4(e)).

Figure 5 shows another depth-encoded 3D visualization of choroid vessels in an eye with pachychoroid disease (Figure 5). This patient is a 19-year-old man with fibrotic changes after chronic CSC with resolved subretinal fluid. An anomalous drainage pattern is observed at the macula in both Sattler's layer from top view and Haller's layer from the bottom view (Figure 5(a) and (c)).

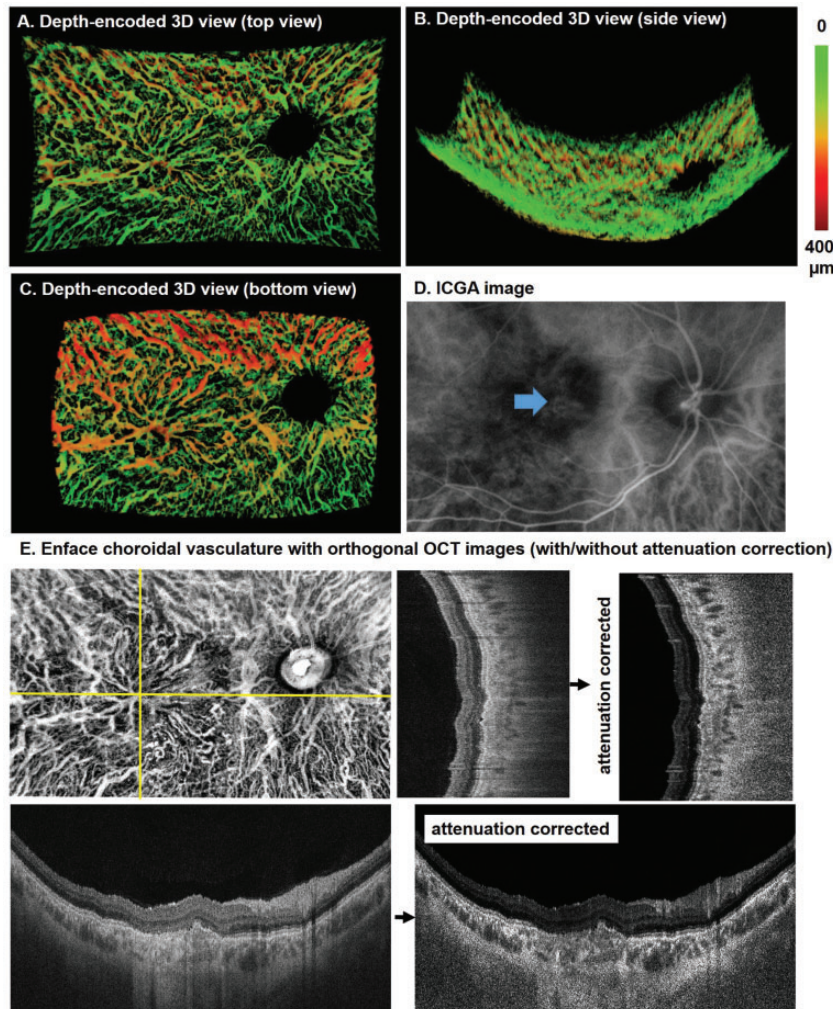


Figure 5. Depth-encoded 3D visualization of the right eye of a 19-year-old male patient with resolved central serous chorioretinopathy. Top view from the vitreous (a), side view from the peripheral retina (b), and bottom view from the sclera (c) of the choroidal vessels segmented from an SS-OCT dataset. (d) The corresponding ICGA image shows shadows at macula (arrow). (e) *En face* choroidal vasculature map with orthogonal SS-OCT images with and without attenuation correction. (A color version of this figure is available in the online journal.)

ICGA: indocyanine green angiography; OCT: optical coherence tomography.

These vessels and their connectivity were poorly visualized on the ICGA (Figure 5(d)) and in the SS-OCT B-scans (Figure 5(e)).

Discussion

The 3D visualizations of the choroidal vasculature described in this work were reconstructed from binarized choroidal vessels segmented from SS-OCT volume scans. This segmentation method has been shown to have good repeatability³⁷ and has been used to quantify choroid thickness and CVI in normal and diseased eyes from other 3D SS-OCT datasets.^{38,41} By representing the choroidal vessel network in 3D, we were able to observe morphological features not appreciated with regional thickness maps or standard measures of CVI. Furthermore, the depth-encoded visualization provided information of choroid thickness and the depth of each vessel below BrM. This information will provide opportunity to better assess the choroid's role in disease mechanisms such as in pachychoroid disease in which compressive effects overlying anteriorly displaced congested veins are believed to induce localized ischemia of the RPE and outer retina.³⁰

By comparing the reconstructed choroidal vessels from SS-OCT with that obtained from ICGA, we found that SS-OCT was able to provide comparable *en face* representations of the choroidal vasculature. Furthermore, the depth-encoded information provided additional features that can distinguish certain vessels of interest. We also found that SS-OCT was able to present choroidal vessels in greater detail compared to ICGA, especially in eyes presenting with profound anatomic alterations affecting dye distribution and visualization of sub-RPE structures, and to identify choroidal vascular structures that were not identified by ICGA, which could represent non-perfused vessels.

Although 3D visualization of choroidal vessels has been explored using SD-OCT and SS-OCT previously, most studies analyzed views from vitreous or sclera.^{27,31,32,34–36,42,43} By encoding the distance to BrM for each vessel, we were able to distinguish the large choroidal vessels in deeper choroid layers especially in eyes with thick choroids. This feature should provide better assessment of choroid in eyes where choroid is significantly thickened by diseases such as CSC.⁴⁴ In addition, we found that the side view of the entire volume revealed features such as regional curvature of the surfaces of BrM and sclera which should be useful to assess pathologies such as choroidal tumors and myopic degeneration.

There are some limitations of this work. Firstly, the *en face* choroidal vasculature was compared with that from ICGA qualitatively. Quantitative analysis is challenging because the vessel segmentations from either OCT images or ICGA images would depend on image resolution and binarization thresholding. We manually overlaid the skeleton of major vessels and observed consistency of both imaging methodologies. Secondly, we reported features of the depth-encoded 3D visualization of choroidal vessels based on limited number of cases. Advantages and disadvantages of this 3D visualization method remain to be explored in more eyes with various pathologies.

Conclusions

We successfully segmented the choroidal vessels from the 3D OCT dataset and color-coded the distance to BrM on the surface of choroidal vessels. The choroidal vasculatures extracted from SS-OCT were compared with those from ICGA and showed comparable patterns of vessel network. Moreover, the 3D network generated from SS-OCT was able to simultaneously provide choroid thickness and vessel depth below BrM information which should prove useful for the study of choroid-related disease.

AUTHORS' CONTRIBUTIONS

All authors participated in the design, interpretation of the studies and analysis of the data and review of the manuscript. TB conducted the patient enrollment and image acquiring; HZ conducted the image processing and data analysis; HZ and RKW wrote the manuscript.


DECLARATION OF CONFLICTING INTERESTS

The author(s) declared the following potential conflicts of interest with respect to the research, authorship, and/or publication of this article: KBF is a consultant for Optovue, Zeiss, Allergan, Genentech, Heidelberg Engineering, Novartis, and Roche. RKW discloses intellectual property owned by the Oregon Health and Science University and the University of Washington. RKW also receives research support from Tasso Inc., Moptim Inc., and Colgate Palmolive Company. He is a consultant to Insight Photonic Solutions and Carl Zeiss Meditec. HZ and TB have no disclosures.

FUNDING

The author(s) disclosed receipt of the following financial support for the research, authorship, and/or publication of this article: This research is supported by grants from the National Eye Institute (R01EY028753), Carl Zeiss Meditec. The funding organization had no role in the design or conduct of this research.

ORCID iD

Hao Zhou  <https://orcid.org/0000-0003-0068-5102>

REFERENCES

- Borrelli E, Sarraf D, Freund KB, Sadda SR. OCT angiography and evaluation of the choroid and choroidal vascular disorders. *Prog Retin Eye Res* 2018;**67**:30–55
- Spaide RF, Ehlers JP, Yiu G. Imaging the choroid: pearls from the experts. *Retina Today* 2013;**Sept**:39–48
- Ring HG, Fujino T. Observations on the anatomy and pathology of the choroidal vasculature. *Arch Ophthalmol* 1967;**78**:431–44
- Olver J. Functional anatomy of the choroidal circulation: methyl methacrylate casting of human choroid. *Eye* 1990;**4**:262–72
- Nickla DL, Wallman J. The multifunctional choroid. *Prog Retin Eye Res* 2010;**29**:144–68
- Singh SR, Vupparaboina KK, Goud A, Dansingani KK, Chhablani J. Choroidal imaging biomarkers. *Surv Ophthalmol* 2019;**64**:312–33
- Campos A, Campos EJ, Martins J, Ambrosio AF, Silva R. Viewing the choroid: where we stand, challenges and contradictions in diabetic retinopathy and diabetic macular oedema. *Acta Ophthalmol* 2017;**95**:446–59

8. Bloome MA. Fluorescein angiography: risks. *Vision Res* 1980;**20**:1083–97
9. Yannuzzi LA, Rohrer KT, Tindel LJ, Sobel RS, Costanza MA, Shields W, Zang E. Fluorescein angiography complication survey. *Ophthalmology* 1986;**93**:611–7
10. Ducrey NM, Delori FC, Gragoudas ES. Monochromatic ophthalmoscopy and fundus photography. II. The pathological fundus. *Arch Ophthalmol* 1979;**97**:288–93
11. Zhang J, Yan Y, Yu ZK, Liu L. Characteristics of polypoidal choroidal vasculopathy evaluated by multispectral imaging. *Ophthalmic Surg Lasers Imaging Retina* 2018;**49**:E249–55
12. Toslak D, Son T, Erol MK, Kim H, Kim TH, Chan RVP, Yao XC. Portable ultra-widefield fundus camera for multispectral imaging of the retina and choroid. *Biomed Opt Express* 2020;**11**:6281–92
13. Takayama K, Ito Y, Kaneko H, Kataoka K, Sugita T, Maruko R, Hattori K, Ra E, Haga F, Terasaki H. Comparison of indocyanine green angiography and optical coherence tomographic angiography in polypoidal choroidal vasculopathy. *Eye* 2017;**31**:45–52
14. Fardeau C, Herbort CP, Kullmann N, Quentel G, LeHoang P. Indocyanine green angiography in birdshot chorioretinopathy. *Ophthalmology* 1999;**106**:1928–34
15. Mrejen S, Spaide RF. Optical coherence tomography: imaging of the choroid and beyond. *Surv Ophthalmol* 2013;**58**:387–429
16. Lavers H, Zambarakji H. Enhanced depth imaging-OCT of the choroid: a review of the current literature. *Graefes Arch Clin Exp Ophthalmol* 2014;**252**:1871–83
17. Choma MA, Sarunic MV, Yang CH, Izatt JA. Sensitivity advantage of swept source and Fourier domain optical coherence tomography. *Opt Express* 2003;**11**:2183–9
18. Drexler W, Fujimoto JG. State-of-the-art retinal optical coherence tomography. *Prog Retin Eye Res* 2008;**27**:45–88
19. Margolis R, Spaide RF. A pilot study of enhanced depth imaging optical coherence tomography of the choroid in normal eyes. *Am J Ophthalmol* 2009;**147**:811–5
20. Maruko I, Iida T, Sugano Y, Ojima A, Ogasawara M, Spaide RF. Subfoveal choroidal thickness after treatment of central serous chorioretinopathy. *Ophthalmology* 2010;**117**:1792–9
21. Chung SE, Kang SW, Lee JH, Kim YT. Choroidal thickness in polypoidal choroidal vasculopathy and exudative age-related macular degeneration. *Ophthalmology* 2011;**118**:840–5
22. Hirata M, Tsujikawa A, Matsumoto A, Hangai M, Ooto S, Yamashiro K, Akiba M, Yoshimura N. Macular choroidal thickness and volume in normal subjects measured by swept-source optical coherence tomography. *Invest Ophthalmol Vis Sci* 2011;**52**:4971–8
23. Jirarattanasopa P, Ooto S, Nakata I, Tsujikawa A, Yamashiro K, Oishi A, Yoshimura N. Choroidal thickness, vascular hyperpermeability, and complement factor H in age-related macular degeneration and polypoidal choroidal vasculopathy. *Invest Ophthalmol Vis Sci* 2012;**53**:3663–72
24. Matri LE, Bouladi M, Chebil A, Kort F, Bouraoui R, Lagueche L, Mghaieth F. Choroidal thickness measurement in highly myopic eyes using SD-OCT. *Ophthalmic Surg Lasers Imaging* 2012;**43**:S38–S43
25. Kirby MA, Li C, Choi WJ, Gregori G, Rosenfeld P, Wang R. Why choroid vessels appear dark in clinical OCT images. In: *Ophthalmic technologies XXVIII: international society for optics and photonics*, 2018, pp.1047428–33.
26. Agrawal R, Gupta P, Tan KA, Cheung CMG, Wong TY, Cheng CY. Choroidal vasculature index as a measure of vascular status of the choroid: measurements in healthy eyes from a population-based study. *Sci Rep* 2016;**6**:1–9
27. Hong Y, Makita S, Yamanari M, Miura M, Kim S, Yatagai T, Yasuno Y. Three-dimensional visualization of choroidal vessels by using standard and ultra-high resolution scattering optical coherence angiography. *Opt Express* 2007;**15**:7538–50
28. Preim B, Oeltze S. *3D visualization of vasculature: an overview*. Berlin, Heidelberg: Springer, 2008, pp.39–59.
29. Gallego-Pinazo R, Dolz-Marco R, Gomez-Ulla F, Mrejen S, Freund KB. Pachychoroid diseases of the macula. *Med Hypothesis Discov Innov Ophthalmol* 2014;**3**:111–5
30. Cheung CMG, Lee WK, Koizumi H, Dansingani K, Lai TYY, Freund KB. Pachychoroid disease. *Eye (Lond)* 2019;**33**:14–33
31. Esmaelpour M, Povazay B, Hermann B, Hofer B, Kajic V, Kapoor K, Sheen NJL, North RV, Drexler W. Three-dimensional 1060-nm OCT: choroidal thickness maps in normal subjects and improved posterior segment visualization in cataract patients. *Invest Ophthalmol Vis Sci* 2010;**51**:5260–6
32. Kajic V, Esmaelpour M, Glittenberg C, Kraus MF, Honegger J, Othara R, Binder S, Fujimoto JG, Drexler W. Automated three-dimensional choroidal vessel segmentation of 3D 1060 nm OCT retinal data. *Biomed Opt Express* 2013;**4**:134–50
33. Duan L, Hong YJ, Yasuno Y. Automated segmentation and characterization of choroidal vessels in high-penetration optical coherence tomography. *Opt Express* 2013;**21**:15787–808
34. Vupparaboina K, Chandra T, Jana S, Richhariya A, Chhablani J. 3D visualization and mapping of choroid thickness based on optical coherence tomography: a step-by-step geometric approach. In: *2013 International conference on 3D imaging*, 2013, pp.1–8.
35. Sekiryu T, Sugano Y, Ojima A, Mori T, Furuta M, Okamoto M, Eifuku S. Hybrid three-dimensional visualization of choroidal vasculature imaged by swept-source optical coherence tomography. *Transl Vis Sci Technol* 2019;**8**:31
36. Tan B, Wong DWK, Yow AP, Yao X, Schmetterer L. Three-dimensional choroidal vessel network quantification using swept source optical coherence tomography. In: *42nd Annual international conference of the IEEE engineering in medicine & biology society (EMBC)*, 2020, pp.1883–6.
37. Zhou H, Chu Z, Zhang Q, Dai Y, Gregori G, Rosenfeld PJ, Wang RK. Attenuation correction assisted automatic segmentation for assessing choroidal thickness and vasculature with swept-source OCT. *Biomed Opt Express* 2018;**9**:6067–80
38. Zhou H, Dai Y, Shi Y, Russell JF, Lyu C, Noorikolouri J, Feuer WJ, Chu Z, Zhang Q, de Sisternes L, Durbin MK, Gregori G, Rosenfeld PJ, Wang RK. Age-related changes in choroidal thickness and the volume of vessels and stroma using swept-source OCT and fully automated algorithms. *Ophthalmol Retina* 2020;**4**:204–15
39. Zhang Q, Huang Y, Zhang T, Kubach S, An L, Laron M, Sharma U, Wang RK. Wide-field imaging of retinal vasculature using optical coherence tomography-based microangiography provided by motion tracking. *J Biomed Opt* 2015;**20**:066008
40. Pizer SM, Amburn EP, Austin JD, Cromartie R, Geselowitz A, Greer T, Terhaarromeny B, Zimmerman JB, Zuiderveld K. Adaptive histogram equalization and its variations. *Comput Vision Graph* 1987;**39**:355–68
41. Shi Y, Zhang Q, Zhou H, Wang L, Chu Z, Jiang X, Shen M, Thulliez M, Lyu C, Feuer W, de Sisternes L, Durbin MK, Gregori G, Wang RK, Rosenfeld PJ. Correlations between choriocapillaris and choroidal measurements and the growth of geographic atrophy using swept source OCT imaging. *Am J Ophthalmol* 2021;**224**:321–31
42. Maloca P, Gyger C, Schoetzau A, Hasler PW. Ultra-short-term reproducibility of speckle-noise freed fluid and tissue compartmentalization of the choroid analyzed by standard OCT. *Trans Vis Sci Technol* 2015;**4**:3
43. Zhang L, Lee K, Niemeijer M, Mullins RF, Sonka M, Abramoff MD. Automated segmentation of the choroid from clinical SD-OCT. *Invest Ophthalmol Vis Sci* 2012;**53**:7510–19
44. Kim YT, Kang SW, Bai KH. Choroidal thickness in both eyes of patients with unilaterally active central serous chorioretinopathy. *Eye* 2011;**25**:1635–40

(Received April 28, 2021, Accepted June 10, 2021)